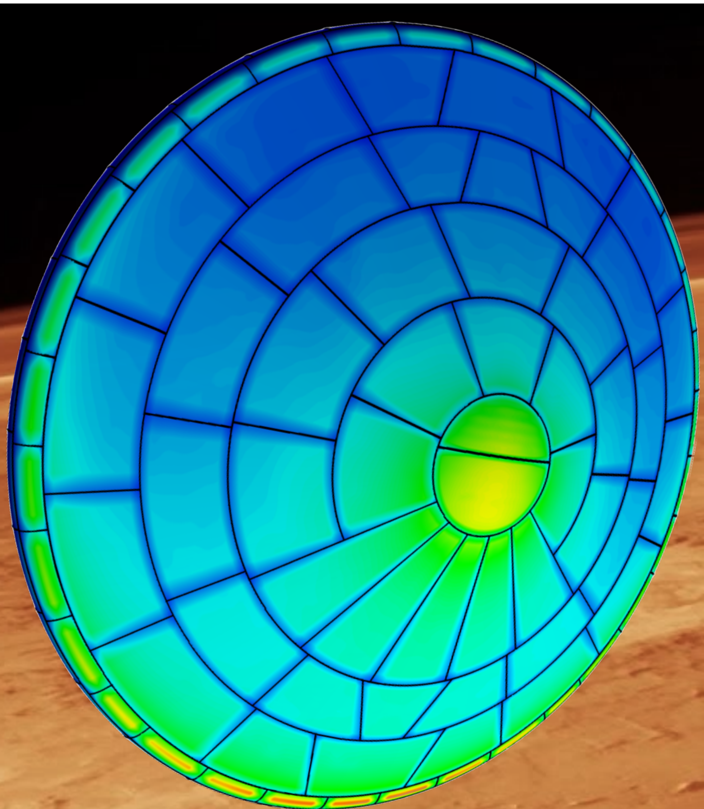

Full-scale Mars Science Laboratory Tiled Heatshield Material Response

9th Ablation Workshop

Montana State University, August 30th - 31st, 2017

Jeremie B. E. Meurisse[1]
Jean Lachaud[2]
Chun Y. Tang[3]
Nagi N. Mansour[3]

[1] Science & Technology Corporation at NASA Ames Research Center, Moffett Field, CA 94035, USA
[2] C la Vie, Nouméa, 98000, New Caledonia.
[3] NASA Ames Research Center, Moffett Field, CA 94035, USA

Overview – Geometry from literature

MSL PICA heatshield

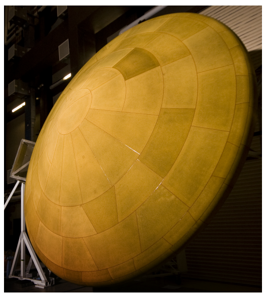

From literature

Aeroshell geometry [1]

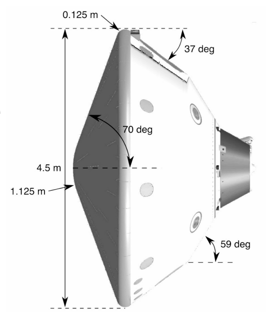

LEGEND

Literature

Overview – Aerothermal environment

MSL PICA heatshield

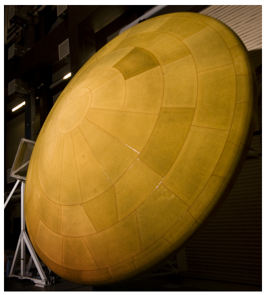

From literature

Aeroshell geometry [1]

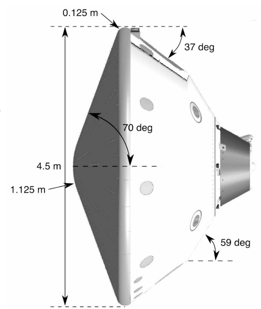

Environment meshing POINTWISE

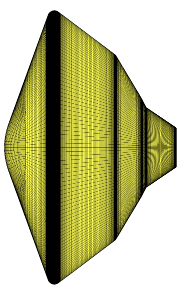

Environment mesh

Hypersonic CFD DPLR [6]

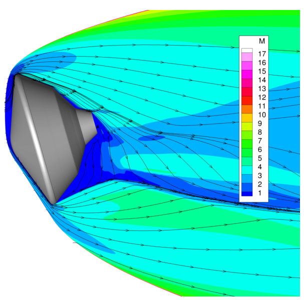

Aerothermal environment around aeroshell

Boundary layer edges BLAYER

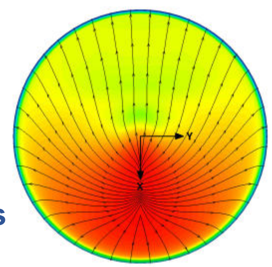

Aerothermal environment at the surface

LEGEND

Literature

Environment

Overview – Material response

MSL PICA heatshield

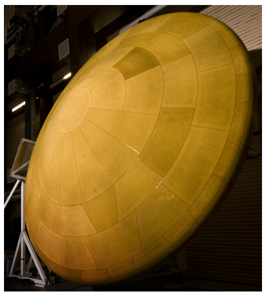

From literature

Aeroshell geometry [1]

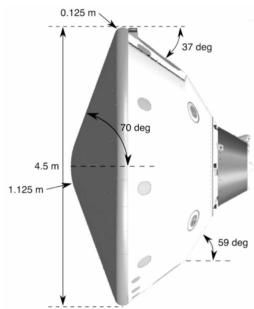

Image processing and material meshing POINTWISE

Material mesh

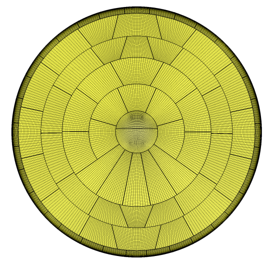

Environment meshing POINTWISE

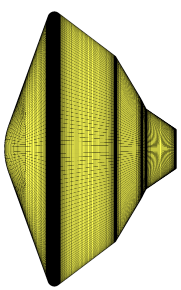

Environment mesh

Hypersonic CFD DPLR [6]

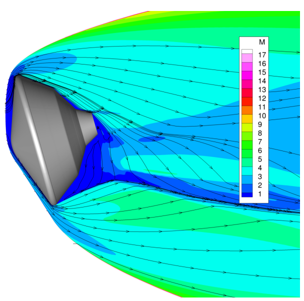

Aerothermal environment around aeroshell

Boundary layer edges BLAYER

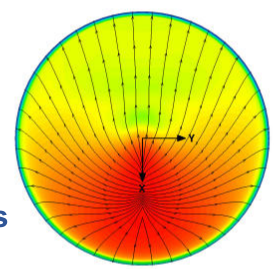

aerothermal environment at the surface

LEGEND

Literature

Environment

Material

Overview – Coupling aerothermal environment and material response

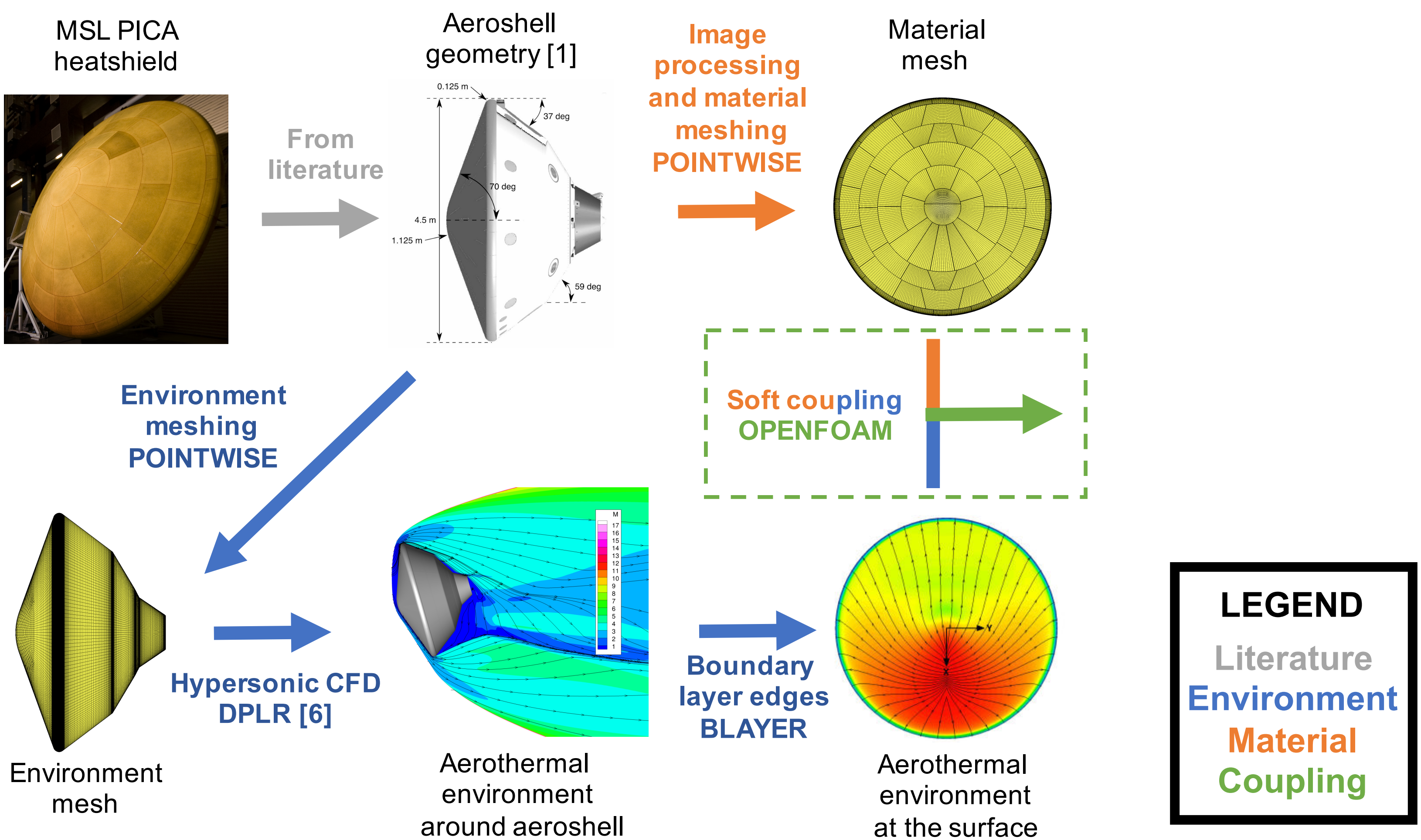

Overview – Coupling aerothermal environment and material response

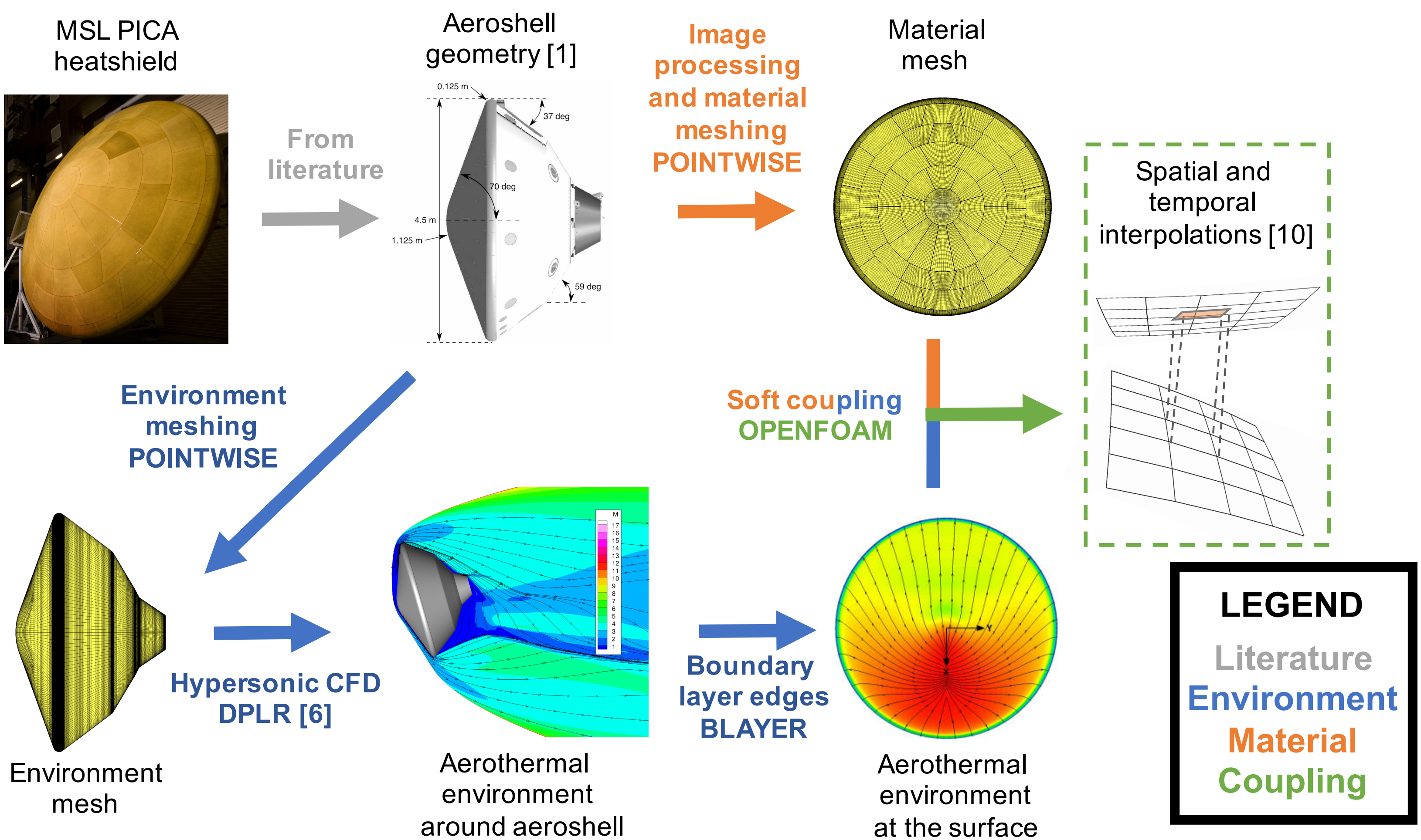

Overview – Coupling aerothermal environment and material response

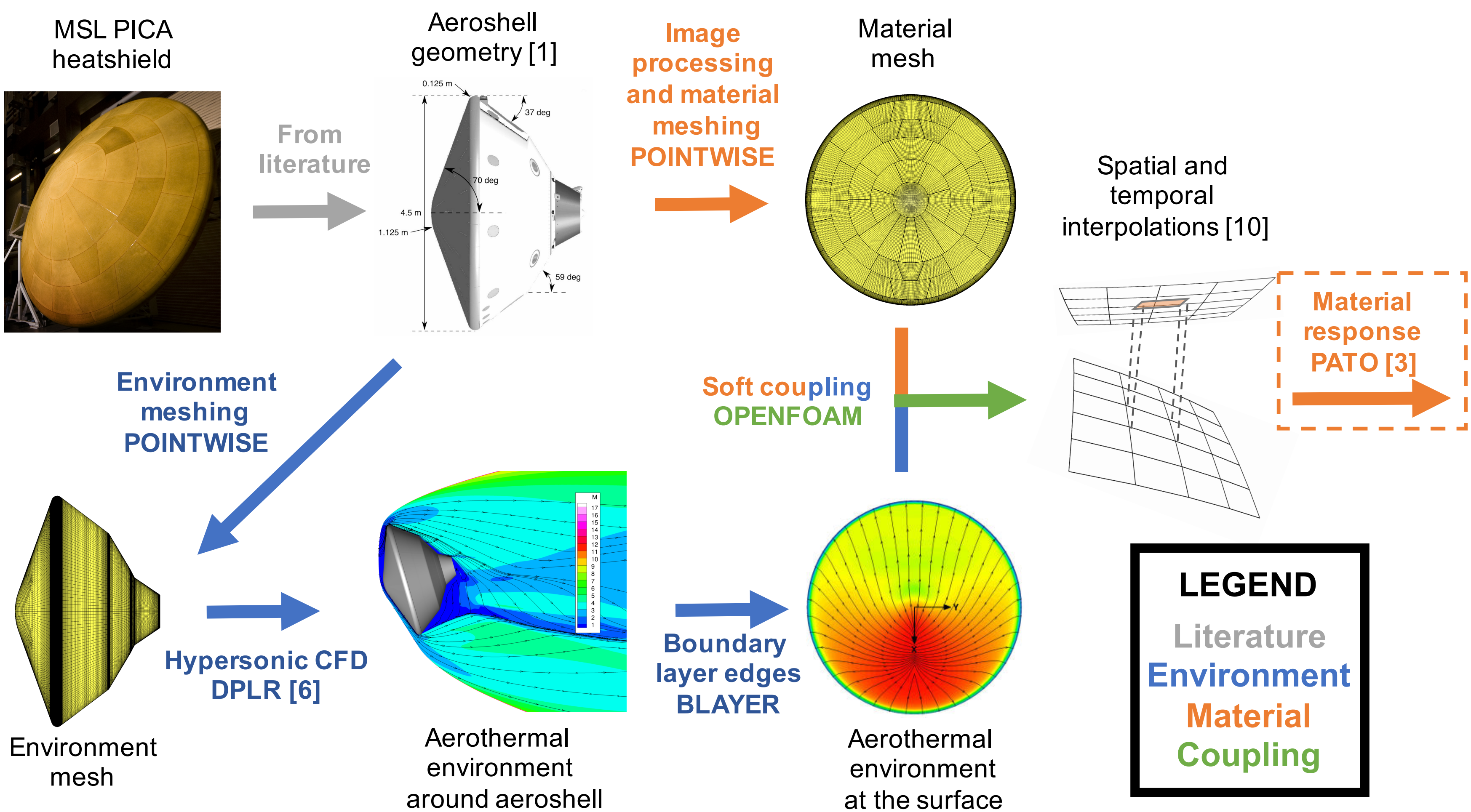

Overview – Coupling aerothermal environment and material response

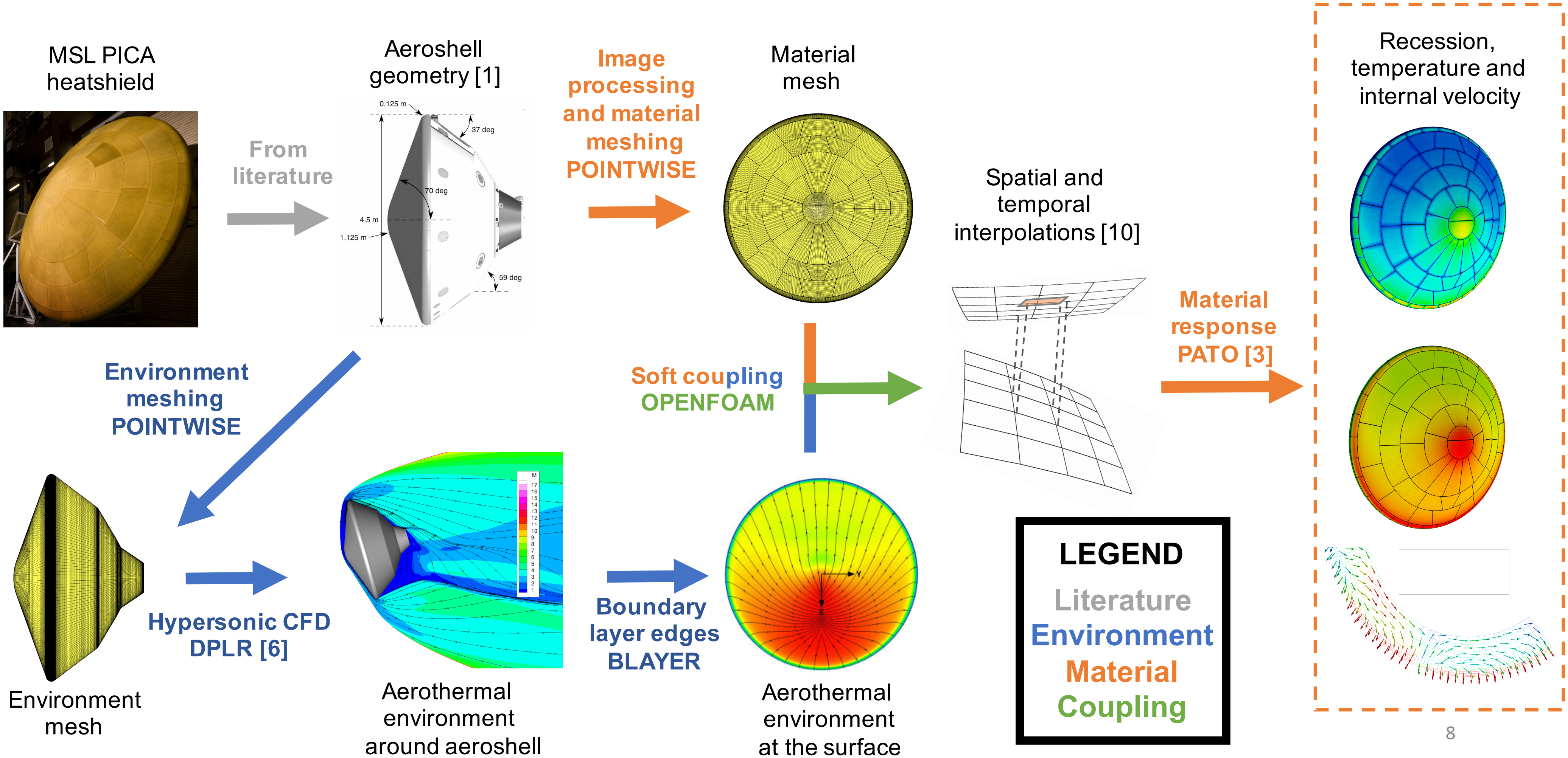

Aerothermal environment computed from DPLR*

DPLR assumptions

- **Laminar** boundary layer
- **Non-blowing** & smooth wall
- Chemical and thermal non-equilibrium
- Radiative equilibrium
- Super-catalytic wall
- Mars atmosphere: y_{CO2} = 0.97, y_{N2} = 0.03
- 12 reactions & 8 species [12]

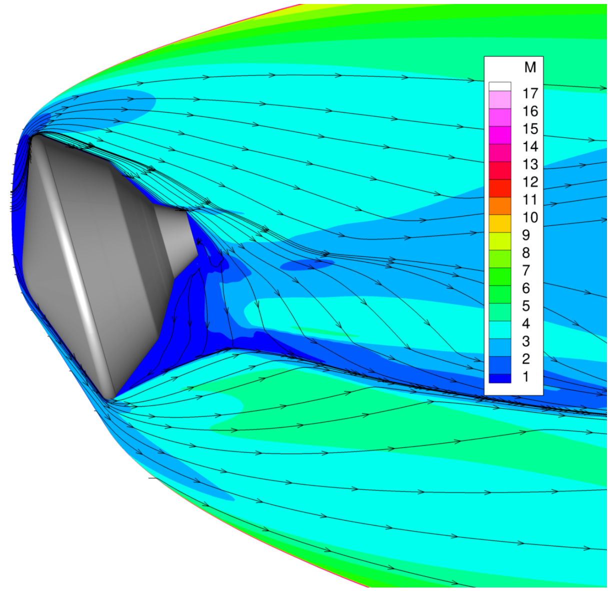

BLAYER calculates the **boundary layer edges** using a curvature-based method

Surface pressure p_w, heat transfer coefficient C_H and **enthalpy h_e** at the **boundary layer edges** are used as inputs in the **material response** code: **PATO**

* DPLR = Data Parallel Line Relaxation [6]

Computational domain of the material response

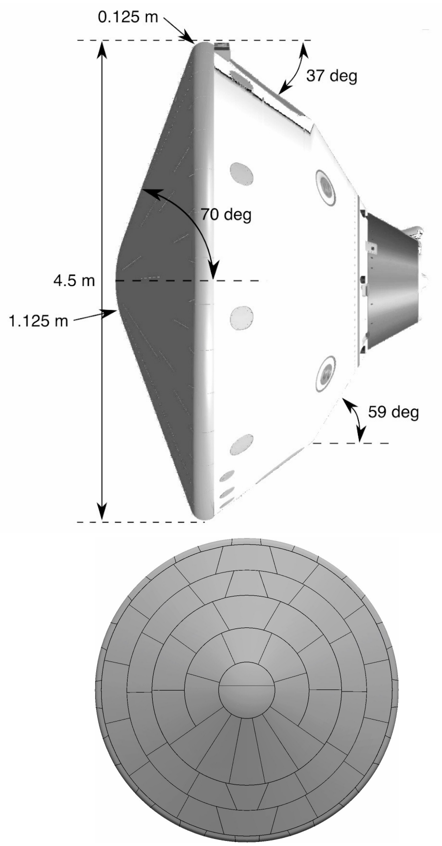

Aeroshell geometry with 113 PICA tiles [1]

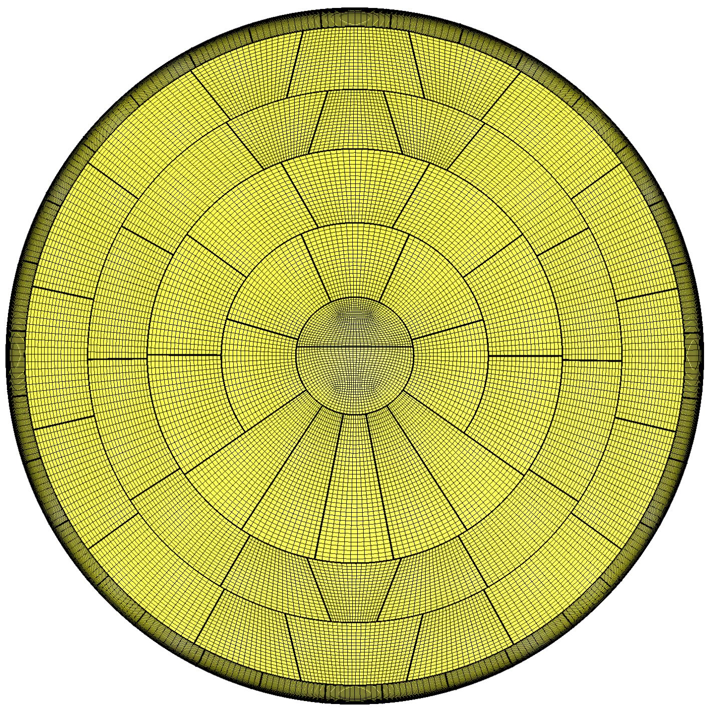

2 million cells mesh of the tiled heatshield

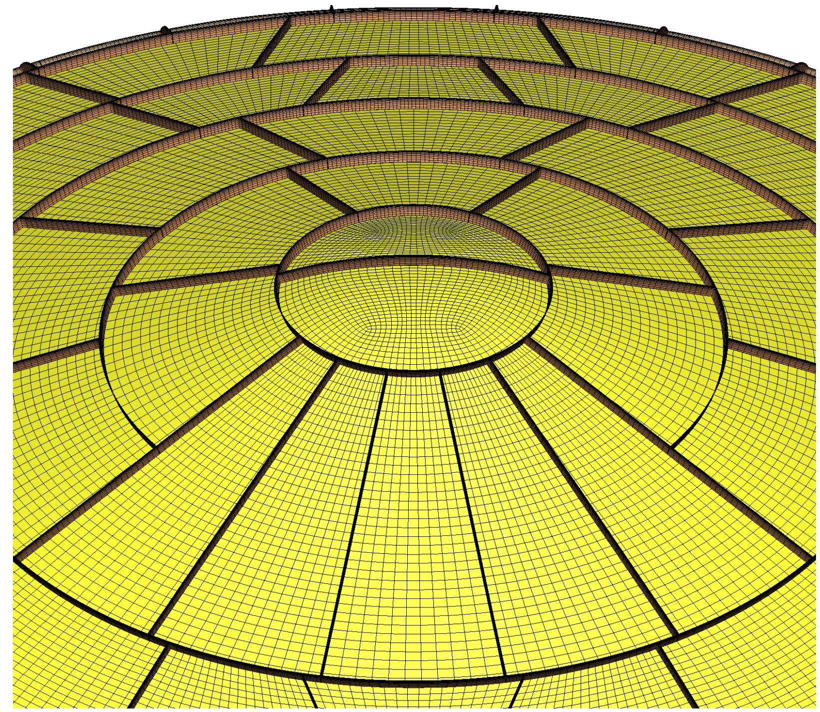

Heatshield material in 2 regions
gap filler + porous tiles

PATO* is used for the material response model

Mass and momentum conservation

$$\boldsymbol{v}_g = -\frac{1}{\epsilon_g}\left(\frac{1}{\mu}\,\overline{\overline{\boldsymbol{K}}} + \frac{1}{p}\,\overline{\overline{\boldsymbol{\beta}}}\right).\,\boldsymbol{\partial}_{\boldsymbol{x}} p_g$$

$$\partial_t \epsilon_g \rho_g \;-\; \boldsymbol{\partial}_{\boldsymbol{x}}\,.\,\left(\epsilon_g \rho_g \boldsymbol{v}_g\right) = \Pi$$

* PATO = Porous material Analysis Toolbox based on OpenFOAM [3]

Open Source Release: http://pato.ac

PATO* is used for the material response model

Mass and momentum conservation

$$\boldsymbol{v}_g = -\frac{1}{\epsilon_g}\left(\frac{1}{\mu}\bar{\bar{\boldsymbol{K}}} + \frac{1}{p}\bar{\bar{\boldsymbol{\beta}}}\right).\,\boldsymbol{\partial}_{\boldsymbol{x}} p_g$$

Permeability [2,11]

$$\partial_t \epsilon_g \rho_g - \boldsymbol{\partial}_{\boldsymbol{x}} \,.\, \left(\epsilon_g \rho_g \boldsymbol{v}_g\right) = \Pi$$

* PATO = Porous material Analysis Toolbox based on OpenFOAM [3]
Open Source Release: http://pato.ac

PATO* is used for the material response model

Mass and momentum conservation

$$\boldsymbol{v}_g = -\frac{1}{\epsilon_g}\left(\frac{1}{\mu}\,\overline{\overline{\boldsymbol{K}}} + \frac{1}{p}\,\overline{\overline{\boldsymbol{\beta}}}\right).\,\boldsymbol{\partial}_{\boldsymbol{x}} p_g$$

Klinkenberg correction [2,11]

$$\partial_t \epsilon_g \rho_g - \boldsymbol{\partial}_{\boldsymbol{x}}\,.\,\left(\epsilon_g \rho_g \boldsymbol{v}_g\right) = \Pi$$

* PATO = Porous material Analysis Toolbox based on OpenFOAM [3]
Open Source Release: http://pato.ac

PATO* is used for the material response model

Mass and momentum conservation

$$\boldsymbol{v}_g = -\frac{1}{\epsilon_g}\left(\frac{1}{\mu}\,\overline{\overline{\boldsymbol{K}}} + \frac{1}{p}\,\overline{\overline{\boldsymbol{\beta}}}\right).\,\boldsymbol{\partial_x} p_g$$

$$\partial_t \epsilon_g \rho_g \; - \; \boldsymbol{\partial_x} \,.\, \left(\epsilon_g \rho_g \boldsymbol{v}_g\right) = \Pi$$

Total pyrolysis-gas production rate [3]

* PATO = Porous material Analysis Toolbox based on OpenFOAM [3]

Open Source Release: http://pato.ac

PATO is used for the material response model

Mass and momentum conservation

$$\boldsymbol{v}_g = -\frac{1}{\epsilon_g}\left(\frac{1}{\mu}\,\overline{\overline{\boldsymbol{K}}} + \frac{1}{p}\,\overline{\overline{\boldsymbol{\beta}}}\right).\,\boldsymbol{\partial}_{\boldsymbol{x}} p_g$$

$$\partial_t \epsilon_g \rho_g \; - \; \boldsymbol{\partial}_{\boldsymbol{x}}\,.\,\left(\epsilon_g \rho_g \boldsymbol{v}_g\right) = \Pi$$

Pyrolysis

$$\partial_t \chi_{i,j} = (\,1 \; - \; \chi_{i,j}\,)^{m_{i,j}}\; T^{n_{i,j}}\; A_{i,j}\; exp\left(\frac{-E_{i,j}}{RT}\right)$$

$$\Pi = \sum_{i=1}^{N_p} \sum_{j=1}^{P_i} \sum_{k=1}^{N_g} \zeta_{i,j,k}\; \epsilon_{i,0}\; \rho_{i,0}\; F_{i,j}\; \partial_t \chi_{i,j}$$

Mass loss and temperature

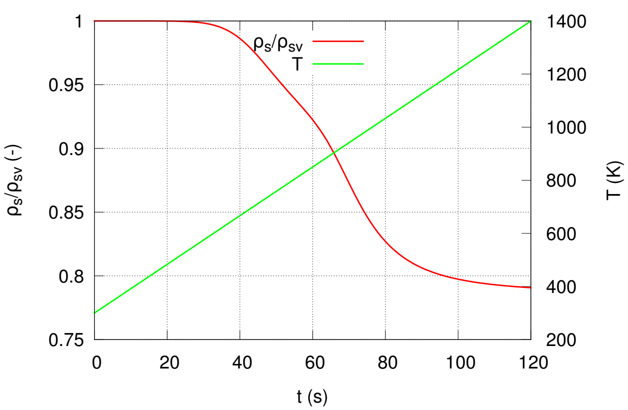

Pyrolysis production rates

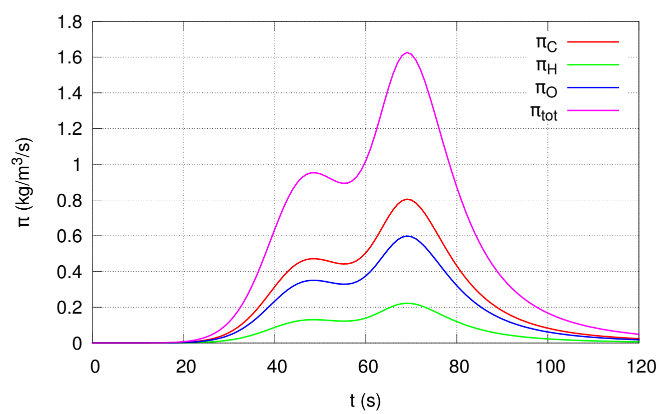

PATO is used for the material response model

Energy conservation

$$\sum_{i=1}^{N_p}\left[\left(\epsilon_i \rho_i c_{p,i}\right) \partial_t T\right] - \boldsymbol{\partial_x} \, . \, \left(\bar{\bar{\boldsymbol{k}}} \, . \, \partial_x T\right) = \sum_{i=1}^{N_p}\left[\, h_i \, \partial_t (\epsilon_i \rho_i) \, \right] - \partial_t\left(\epsilon_g \rho_g h_g - \epsilon_g p_g\right) + \boldsymbol{\partial_x} \, . \left(\epsilon_g \rho_g h_g \boldsymbol{v}_g\right)$$

PATO is used for the material response model

Energy conservation

$$\sum_{i=1}^{N_p}\left[\left(\epsilon_i \rho_i c_{p,i}\right) \partial_t T\right] - \boldsymbol{\partial_x} . \left(\overline{\overline{\boldsymbol{k}}} . \partial_x T\right) = \sum_{i=1}^{N_p}\left[h_i \, \partial_t (\epsilon_i \rho_i) \right] - \partial_t\left(\epsilon_g \rho_g h_g - \epsilon_g p_g\right) + \boldsymbol{\partial_x} . \left(\epsilon_g \rho_g h_g \boldsymbol{v}_g\right)$$

Solid phases storage – implicit in T

PATO is used for the material response model

Energy conservation

$$\sum_{i=1}^{N_p}\left[\left(\epsilon_i\rho_i c_{p,i}\right)\partial_t T\right]\left(-\boldsymbol{\partial_x}\,.\left(\bar{\bar{\boldsymbol{k}}}\,.\,\partial_x T\right)\right)=\sum_{i=1}^{N_p}\left[\,h_i\,\partial_t(\epsilon_i\rho_i)\,\right]-\partial_t\left(\epsilon_g\rho_g h_g-\epsilon_g p_g\right)+\boldsymbol{\partial_x}\,.\left(\epsilon_g\rho_g h_g\boldsymbol{v}_g\right)$$

Conduction – implicit in T

PATO is used for the material response model

Energy conservation

$$\sum_{i=1}^{N_p}\left[\left(\epsilon_i\rho_i c_{p,i}\right)\partial_t T\right] - \boldsymbol{\partial_x} \cdot \left(\overline{\overline{\boldsymbol{k}}} \cdot \partial_x T\right) = \sum_{i=1}^{N_p}\left[\, h_i\, \partial_t(\epsilon_i\rho_i)\,\right] - \partial_t\left(\epsilon_g\rho_g h_g - \epsilon_g p_g\right) + \boldsymbol{\partial_x} \cdot \left(\epsilon_g\rho_g h_g \boldsymbol{v}_g\right)$$

Solid mass loss by pyrolysis and heterogeneous reactions – explicit

PATO is used for the material response model

Energy conservation

$$\sum_{i=1}^{N_p}\left[\left(\epsilon_i\rho_i c_{p,i}\right)\partial_t T\right] - \boldsymbol{\partial_x}\,.\,\left(\overline{\overline{\boldsymbol{k}}}\,.\,\partial_x T\right) = \sum_{i=1}^{N_p}\left[\,h_i\,\partial_t(\epsilon_i\rho_i)\,\right] - \left(\partial_t\left(\epsilon_g\rho_g h_g - \epsilon_g p_g\right)\right) + \boldsymbol{\partial_x}\,.\left(\epsilon_g\rho_g h_g \boldsymbol{v}_g\right)$$

Gas storage – explicit

PATO is used for the material response model

Energy conservation

$$\sum_{i=1}^{N_p}\left[\left(\epsilon_i \rho_i c_{p,i}\right)\partial_t T\right] - \boldsymbol{\partial_x} \cdot \left(\overline{\overline{\boldsymbol{k}}} \cdot \partial_x T\right) = \sum_{i=1}^{N_p}\left[\, h_i\, \partial_t(\epsilon_i \rho_i)\,\right] - \partial_t\left(\epsilon_g \rho_g h_g - \epsilon_g p_g\right) + \boldsymbol{\partial_x} \cdot \left(\epsilon_g \rho_g h_g \boldsymbol{v}_g\right)$$

Convection – explicit

PATO is used for the material response model

Energy conservation

$$\sum_{i=1}^{N_p}\left[\left(\epsilon_i\rho_i c_{p,i}\right)\partial_t T\right] - \boldsymbol{\partial_x}\,.\,\left(\overline{\overline{\boldsymbol{k}}}\,.\,\partial_x T\right) = \sum_{i=1}^{N_p}\left[\,h_i\,\partial_t(\epsilon_i\rho_i)\,\right] - \partial_t\left(\epsilon_g\rho_g h_g - \epsilon_g p_g\right) + \boldsymbol{\partial_x}\,.\left(\epsilon_g\rho_g h_g \boldsymbol{v}_g\right)$$

Isotropic TACOT properties

Virgin and char specific heat

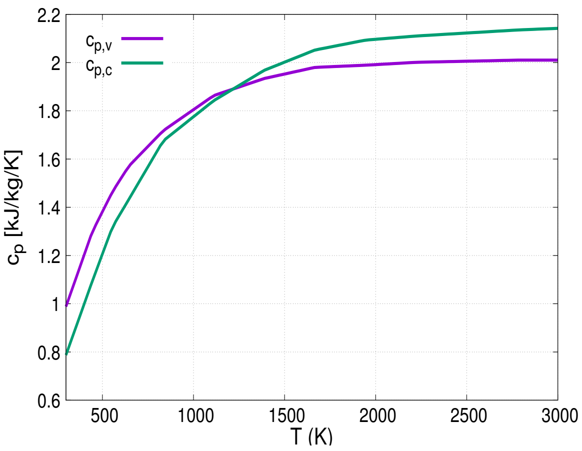

PATO is used for the material response model

Energy conservation

$$\sum_{i=1}^{N_p}\left[\left(\epsilon_i\rho_i c_{p,i}\right)\partial_t T\right] - \boldsymbol{\partial_x}\cdot\left(\bar{\bar{\boldsymbol{k}}}\cdot\partial_x T\right) = \sum_{i=1}^{N_p}\left[\, h_i\,\partial_t(\epsilon_i\rho_i)\,\right] - \partial_t\left(\epsilon_g\rho_g h_g - \epsilon_g p_g\right) + \boldsymbol{\partial_x}\cdot\left(\epsilon_g\rho_g h_g \boldsymbol{v}_g\right)$$

Isotropic TACOT properties

Virgin and char specific heat

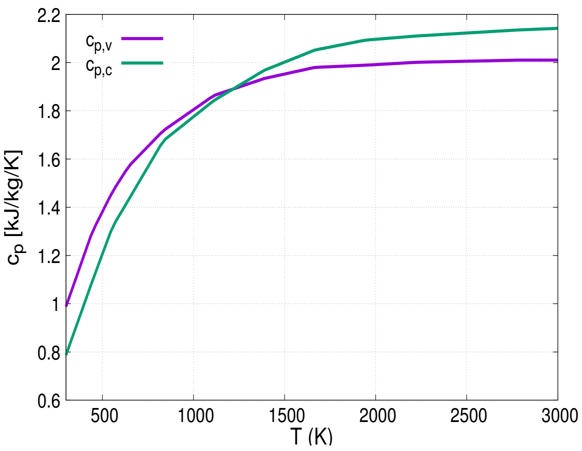

Virgin and char thermal conductivity [13]

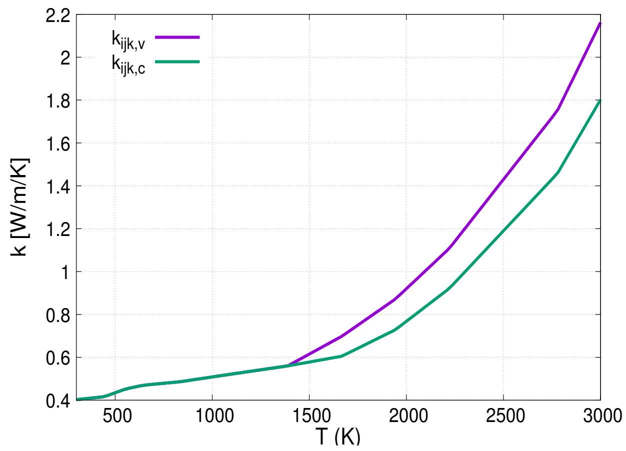

PATO is used for the material response model

Energy conservation

$$\sum_{i=1}^{N_p}\left[\left(\epsilon_i \rho_i c_{p,i}\right) \partial_t T\right] - \boldsymbol{\partial_x} . \left(\bar{\bar{\boldsymbol{k}}} . \partial_x T\right) = \sum_{i=1}^{N_p}\left[h_i \partial_t (\epsilon_i \rho_i) \right] - \partial_t\left(\epsilon_g \rho_g h_g - \epsilon_g p_g\right) + \boldsymbol{\partial_x} . \left(\epsilon_g \rho_g h_g \boldsymbol{v}_g\right)$$

Isotropic TACOT properties

Virgin and char specific heat

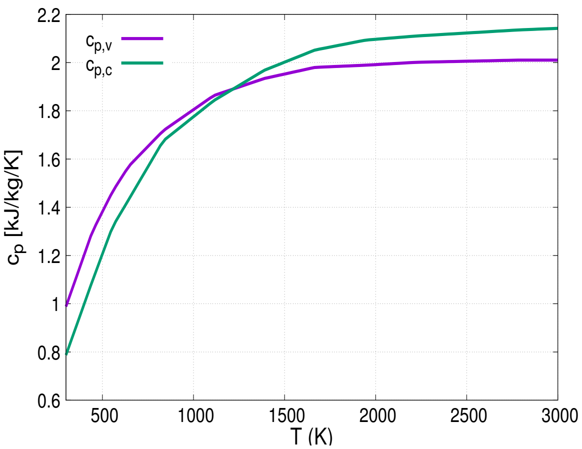

Virgin and char thermal conductivity [13]

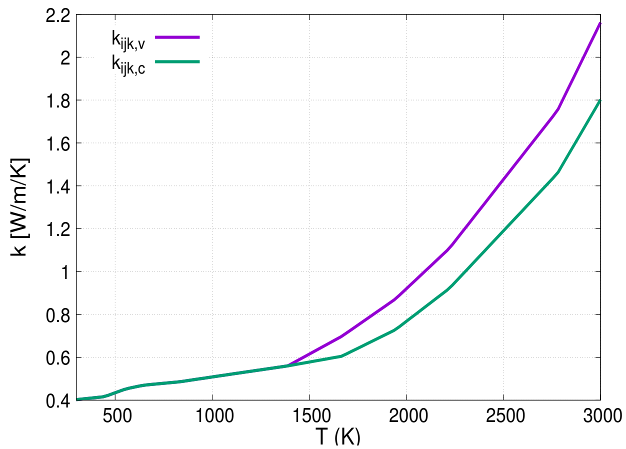

Virgin and char enthalpy

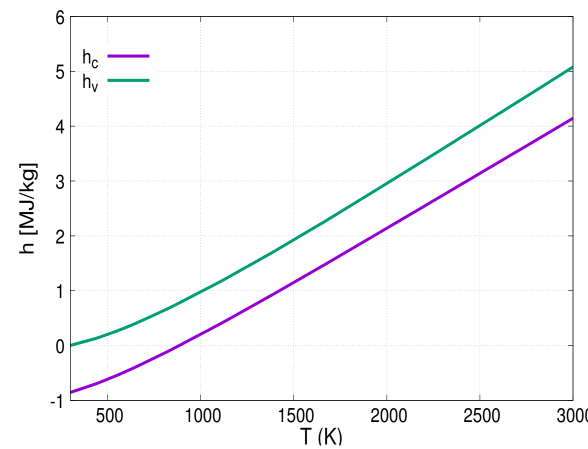

PATO is used for the material response model

Boundary Conditions

Surface mass balance [7]

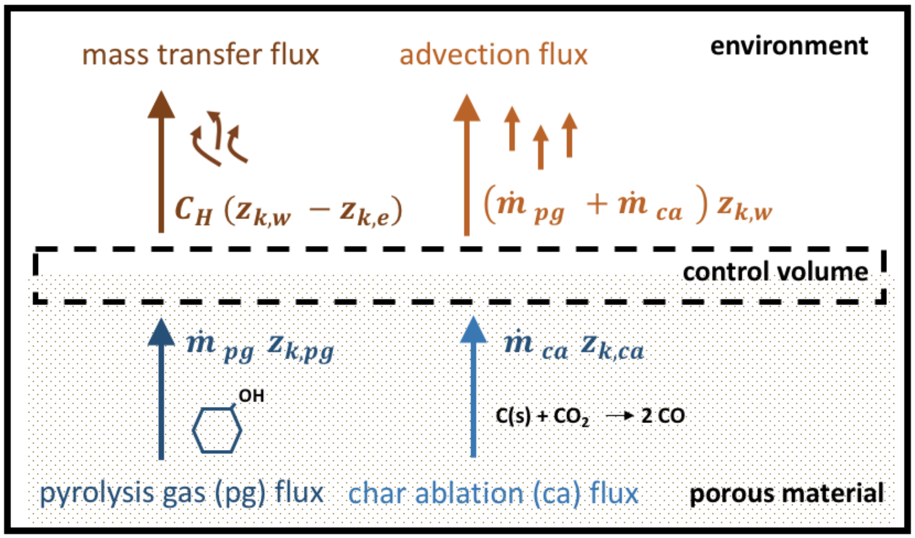

Enthalpy at the wall h_w

Char ablation rate $\dot{m}_{ca}$

PATO is used for the material response model

Boundary Conditions

Surface mass balance [7]

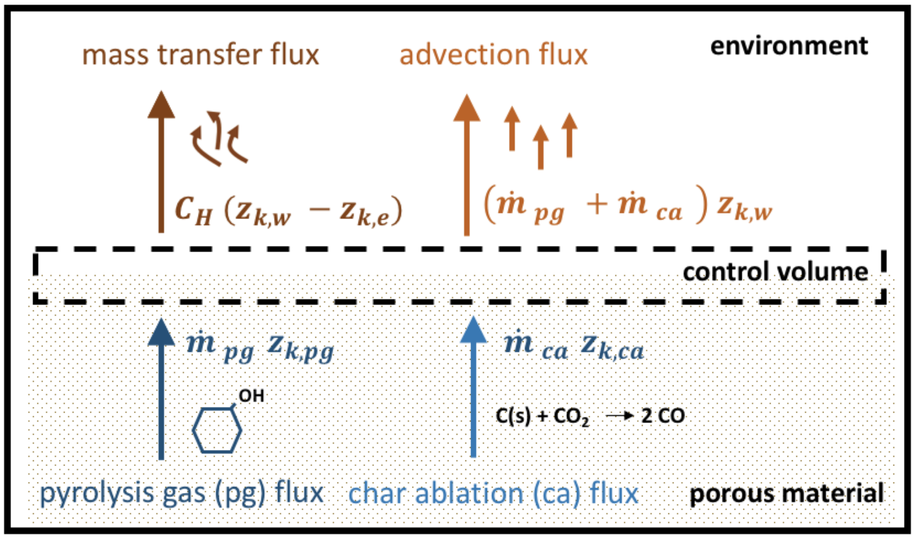

Surface energy balance [8,9]

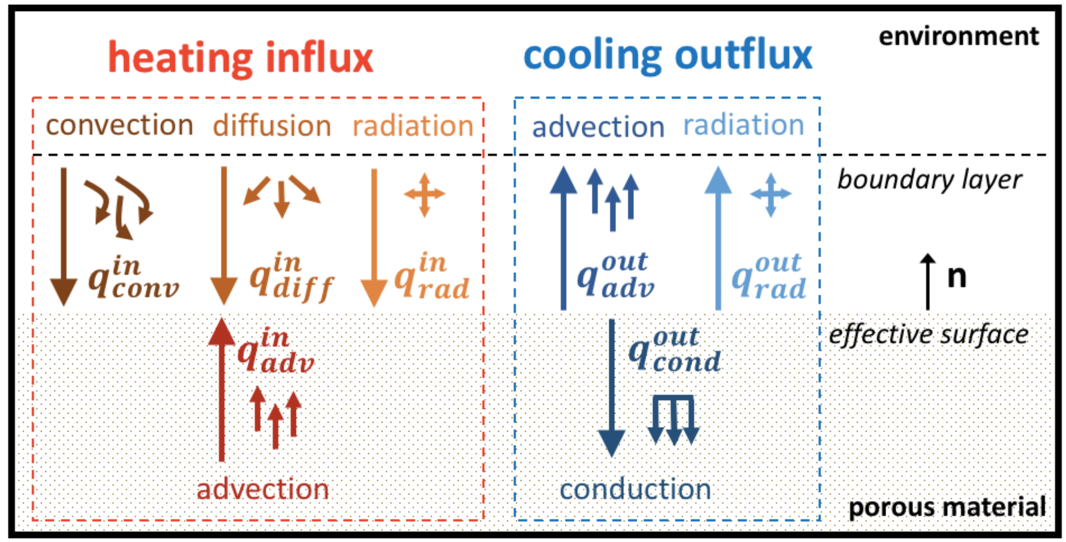

Enthalpy at the wall h_w

Char ablation rate $\dot{m}_{ca}$

Temperature at the wall T_w

Temporal and spatial interpolations

Temporal interpolation

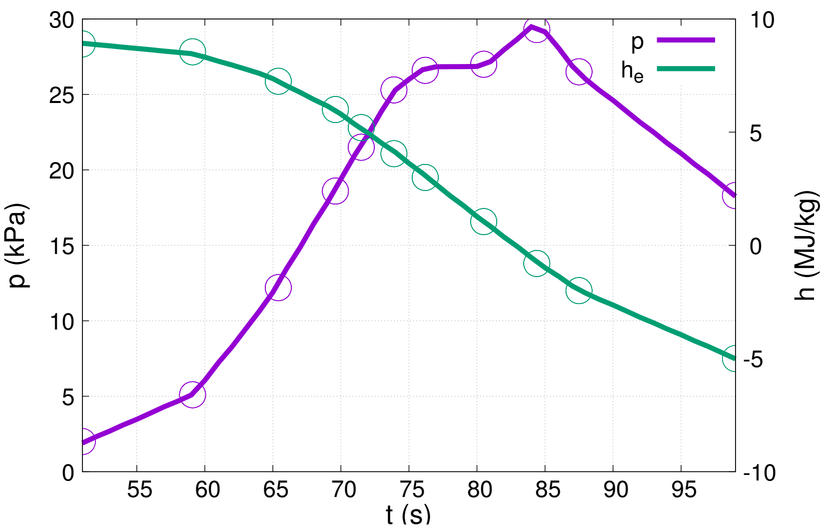

11 **discrete** times
(50s to 100s of MSL entry)
linear interpolation

Spatial interpolation

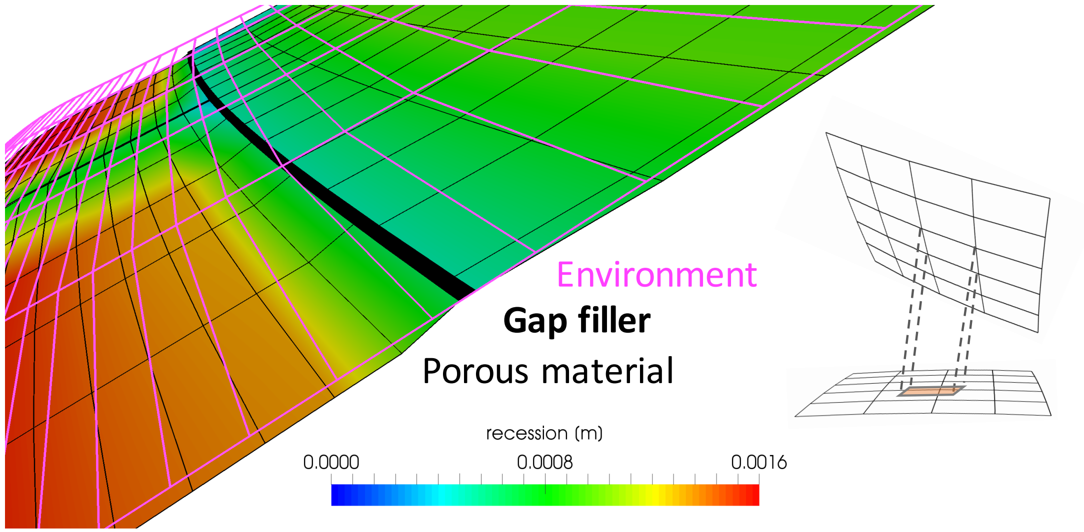

Separate mesh regions are numerically **connected** by the **Arbitrary Mesh Interface** (**AMI**) utility using local **Galerkin projection** [10] implemented in **OpenFOAM**

“Fencing” effect at tile interfaces

Post-test arcjet coupons [5]

Pre Test Sample | 85 W/cm², 0.33 atm | 175 W/cm², 0.28 atm | 270 W/cm², 0.27 atm

“Fencing” effect at tile interfaces

Post-test arcjet coupons [5]

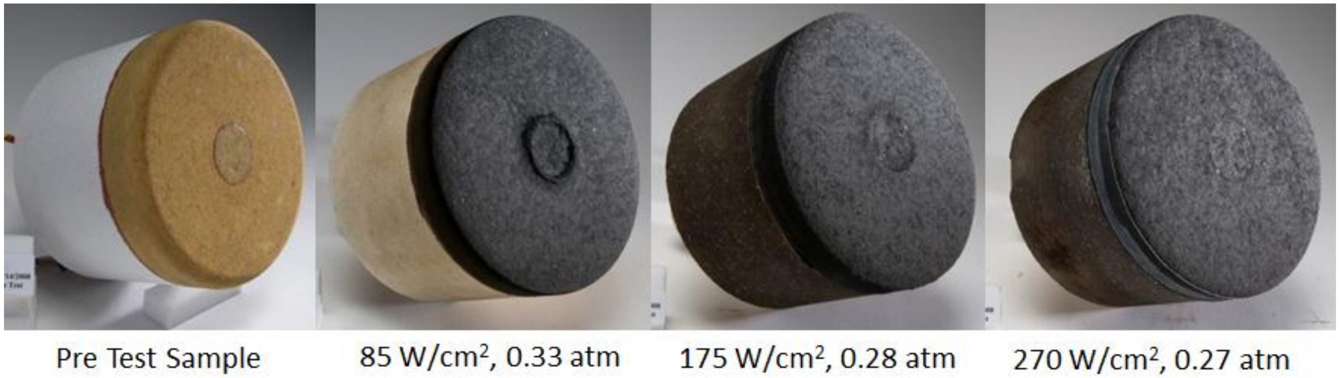

MSL heatshield front surface at the nose

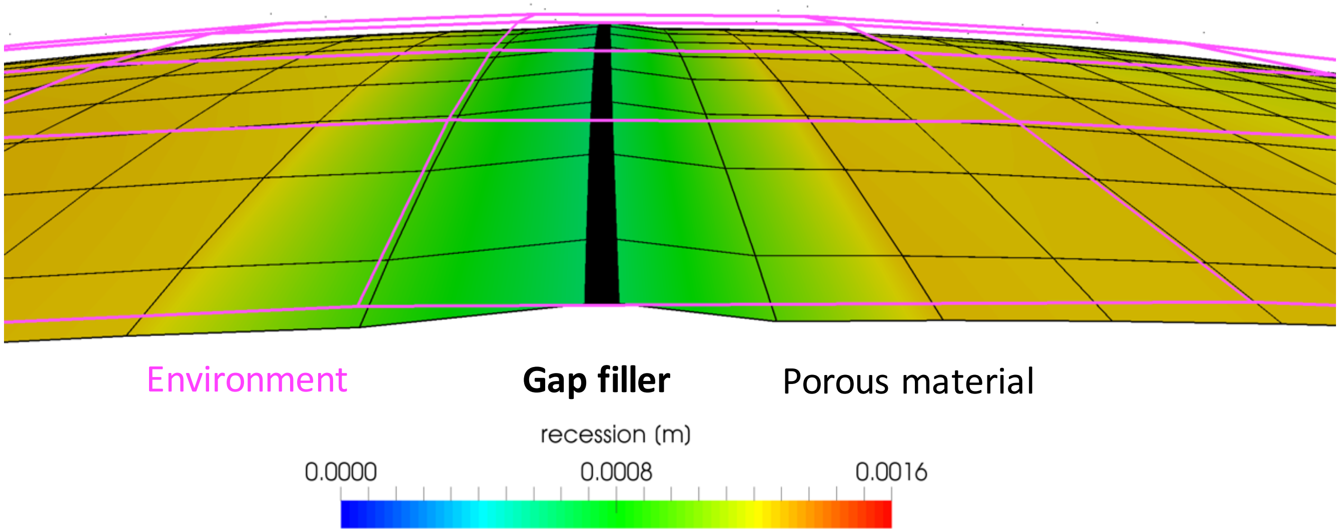

Temperature from PATO

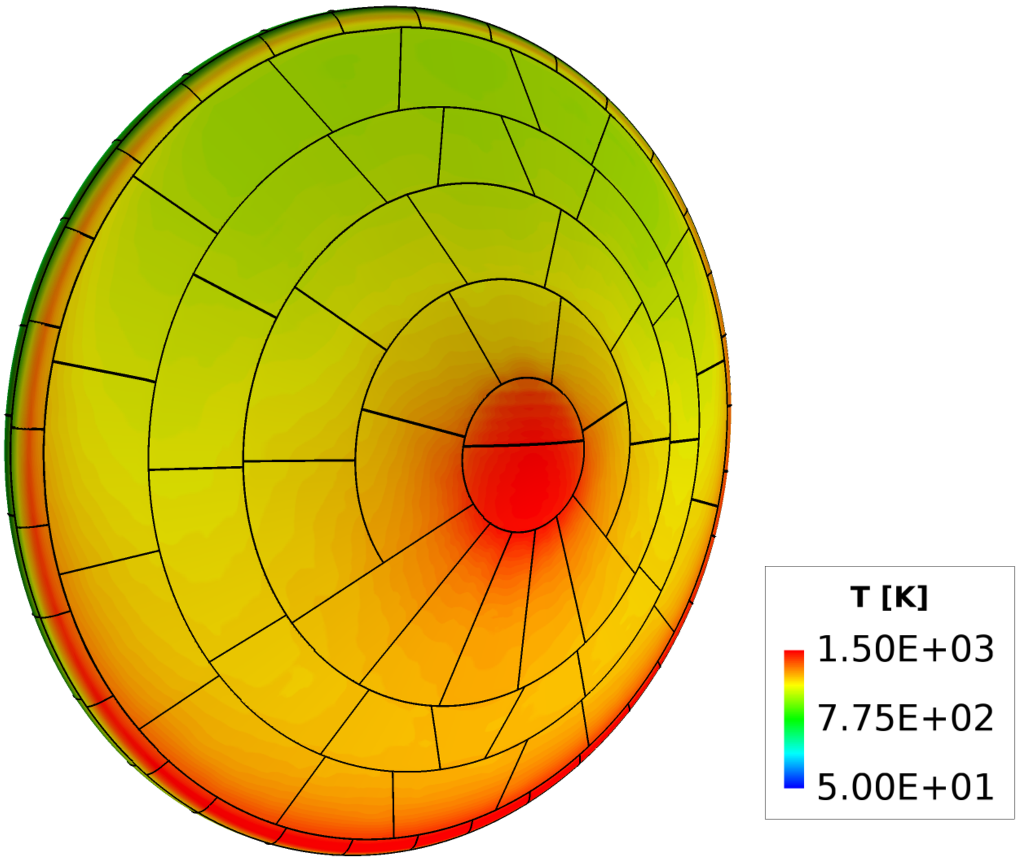

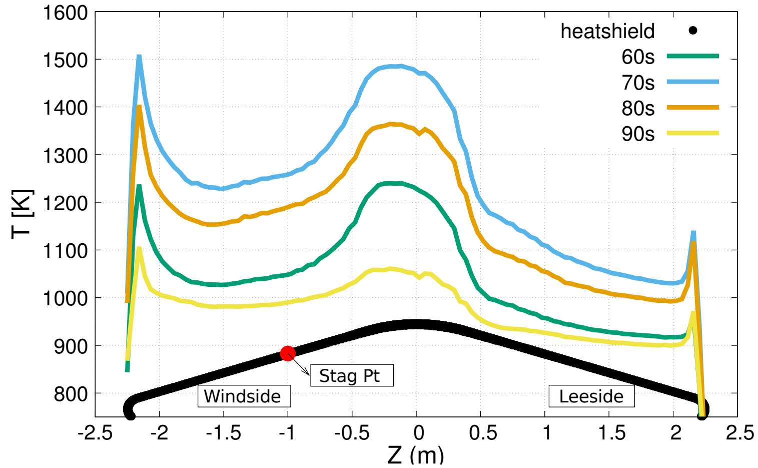

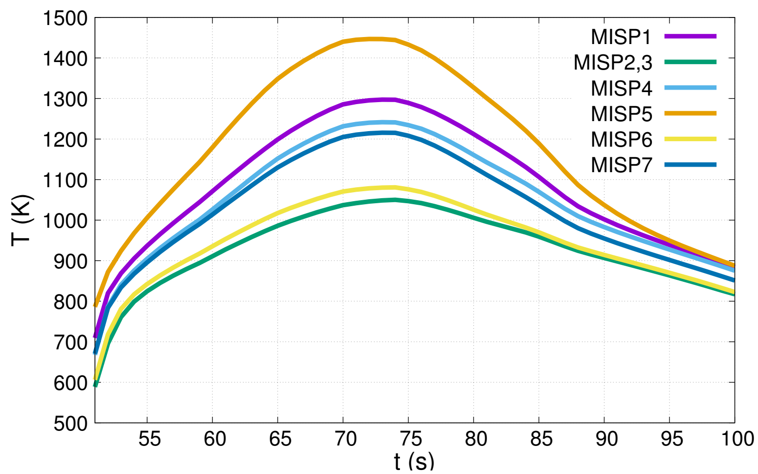

Recession from PATO

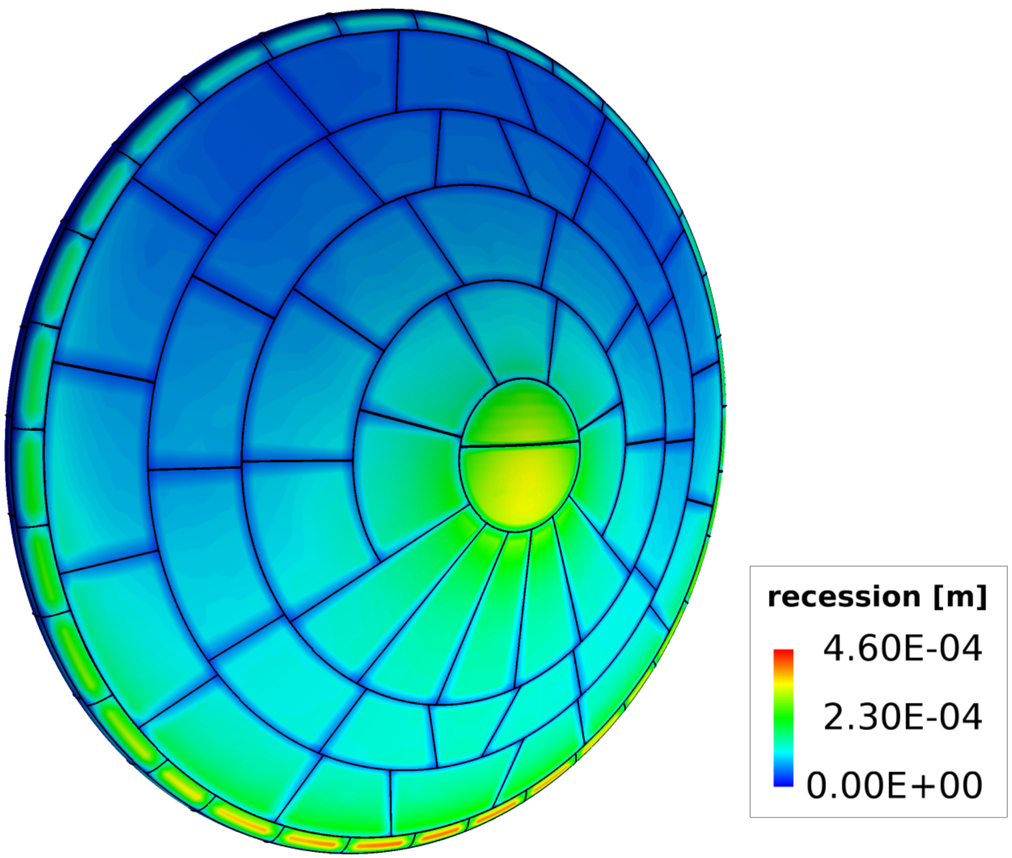

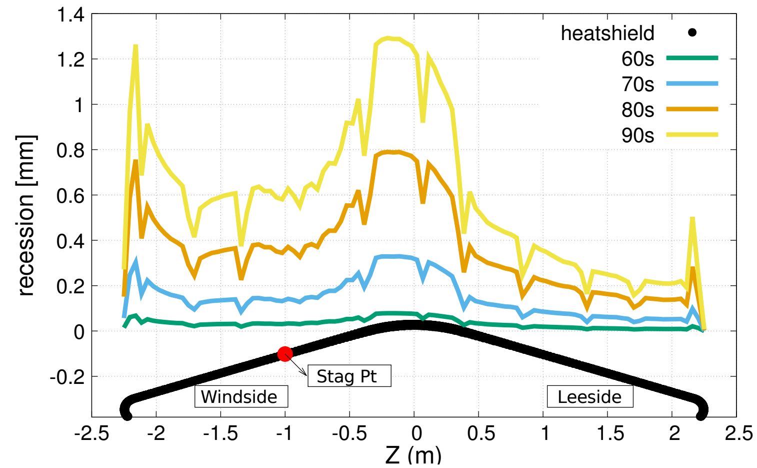

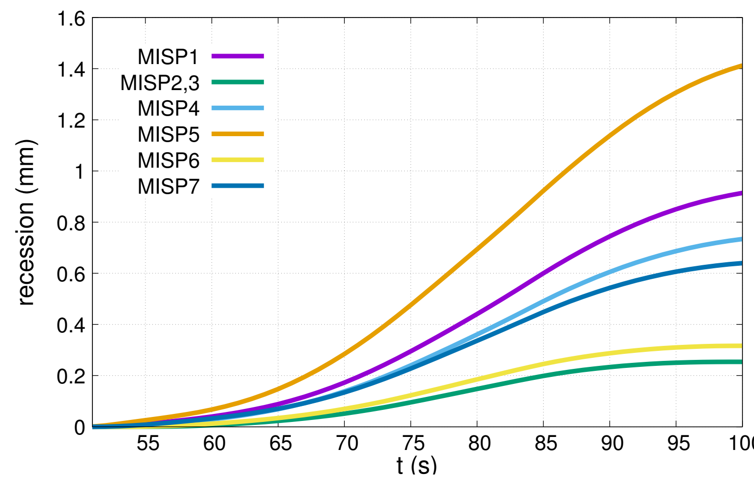

Velocity inside the porous material

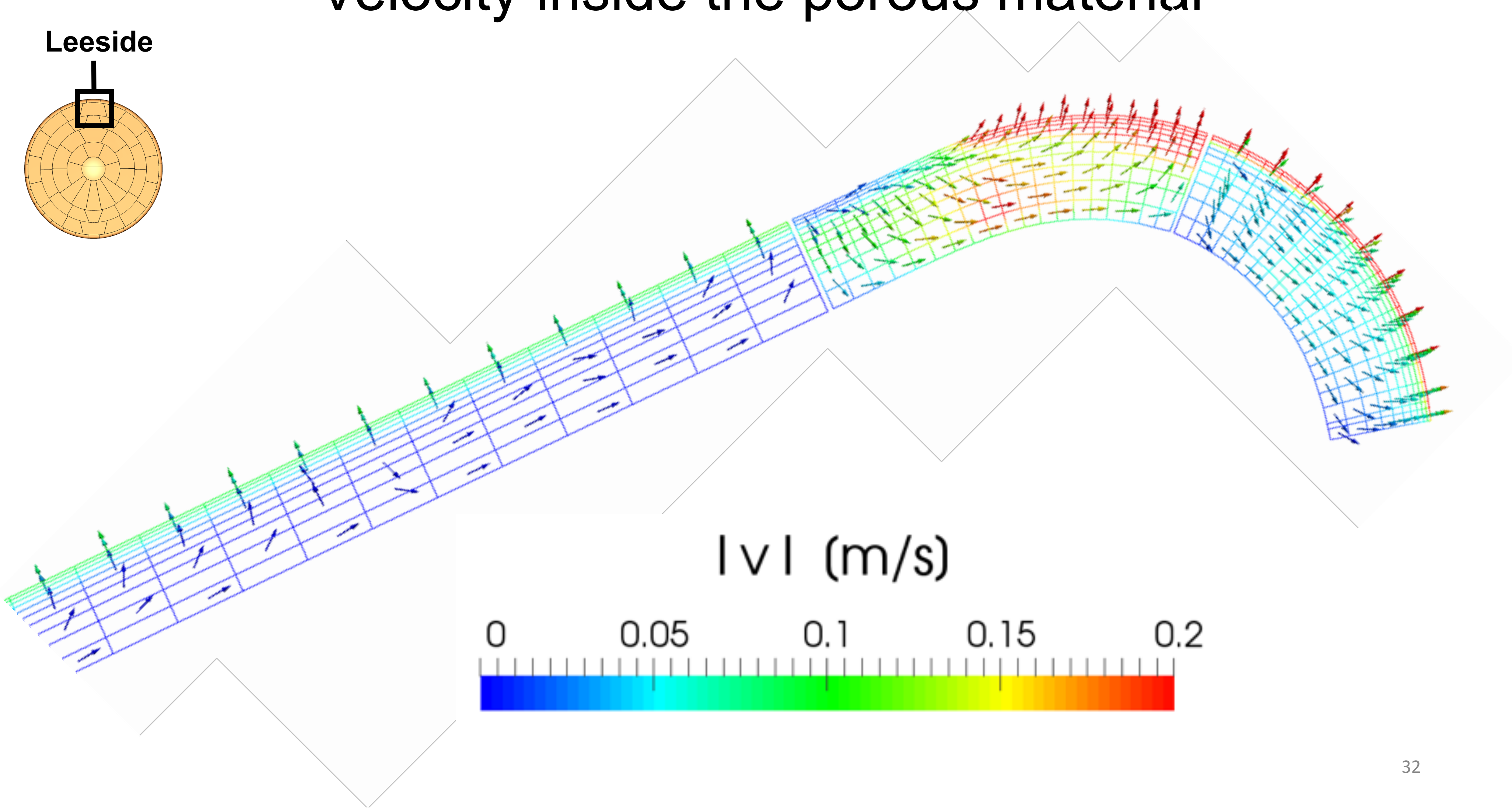

Velocity inside the porous material

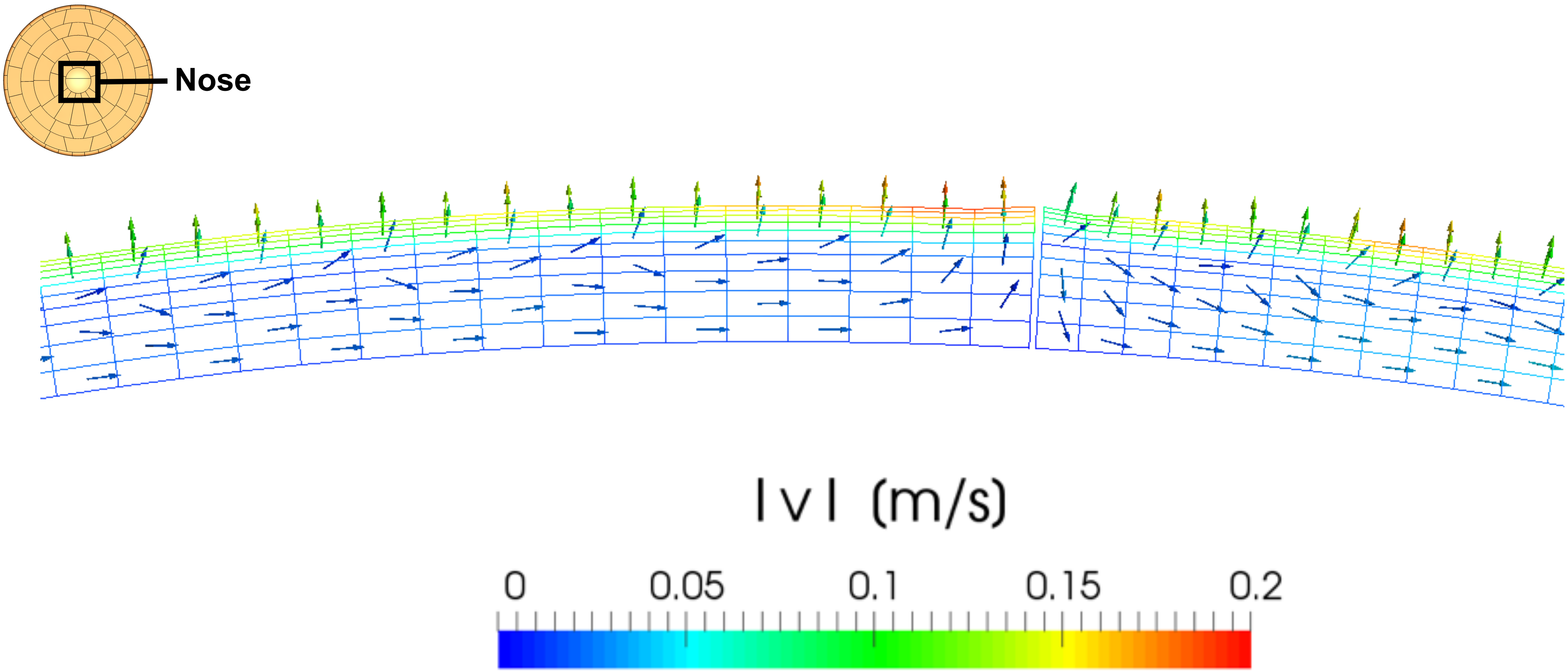

Tiled configuration changes the flow inside the material

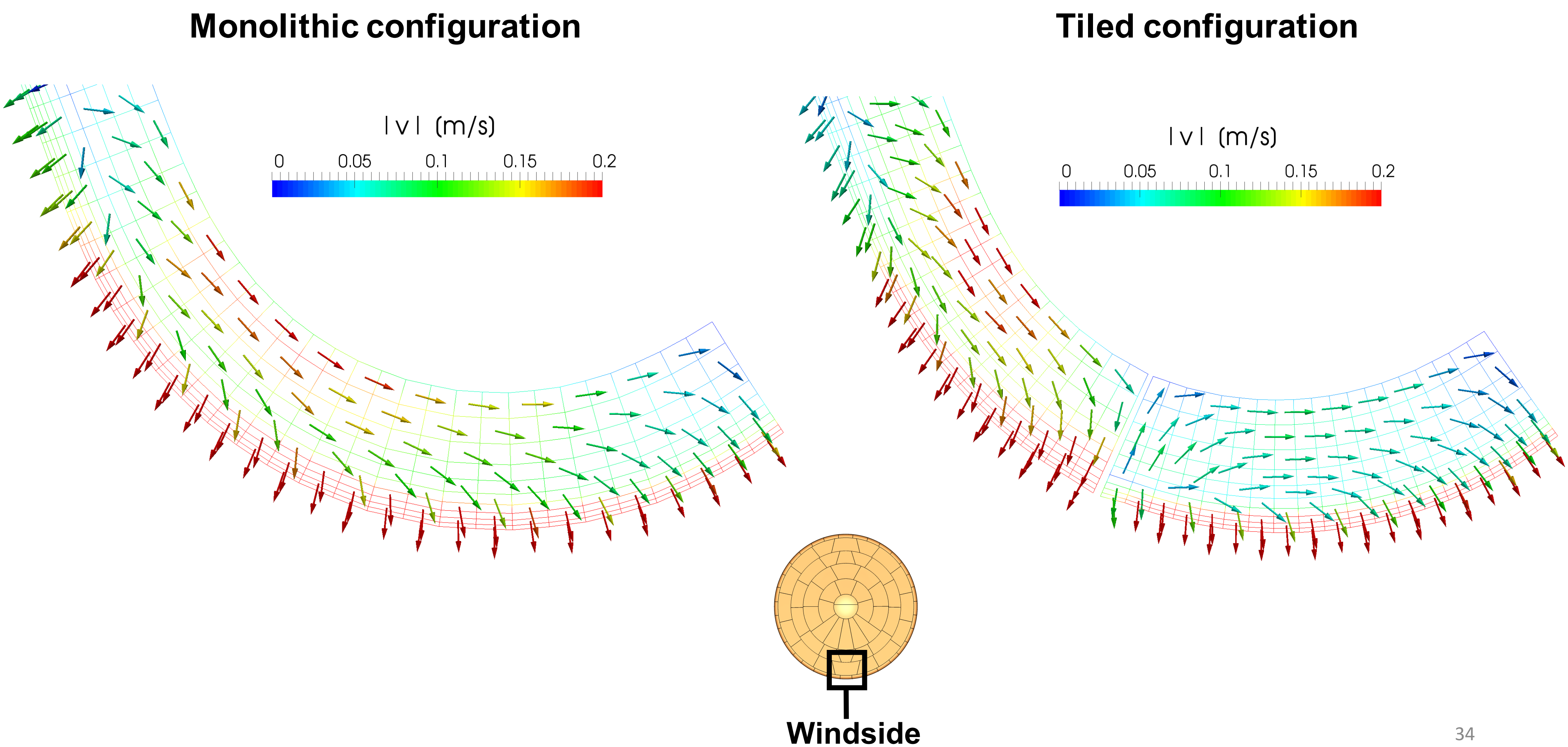

1D and 3D material response comparison – nose

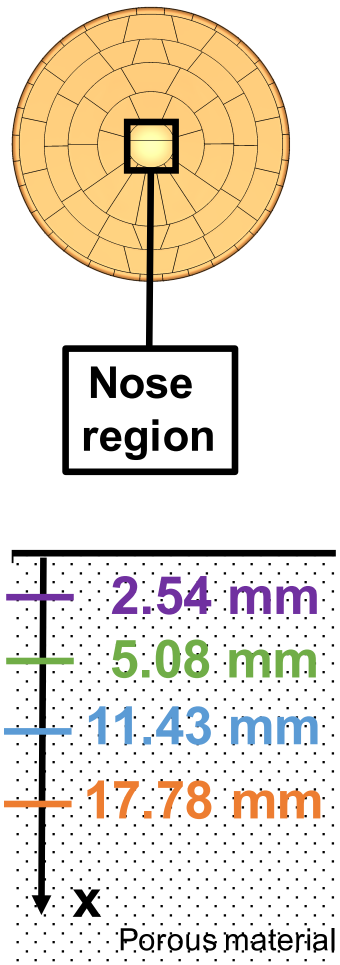

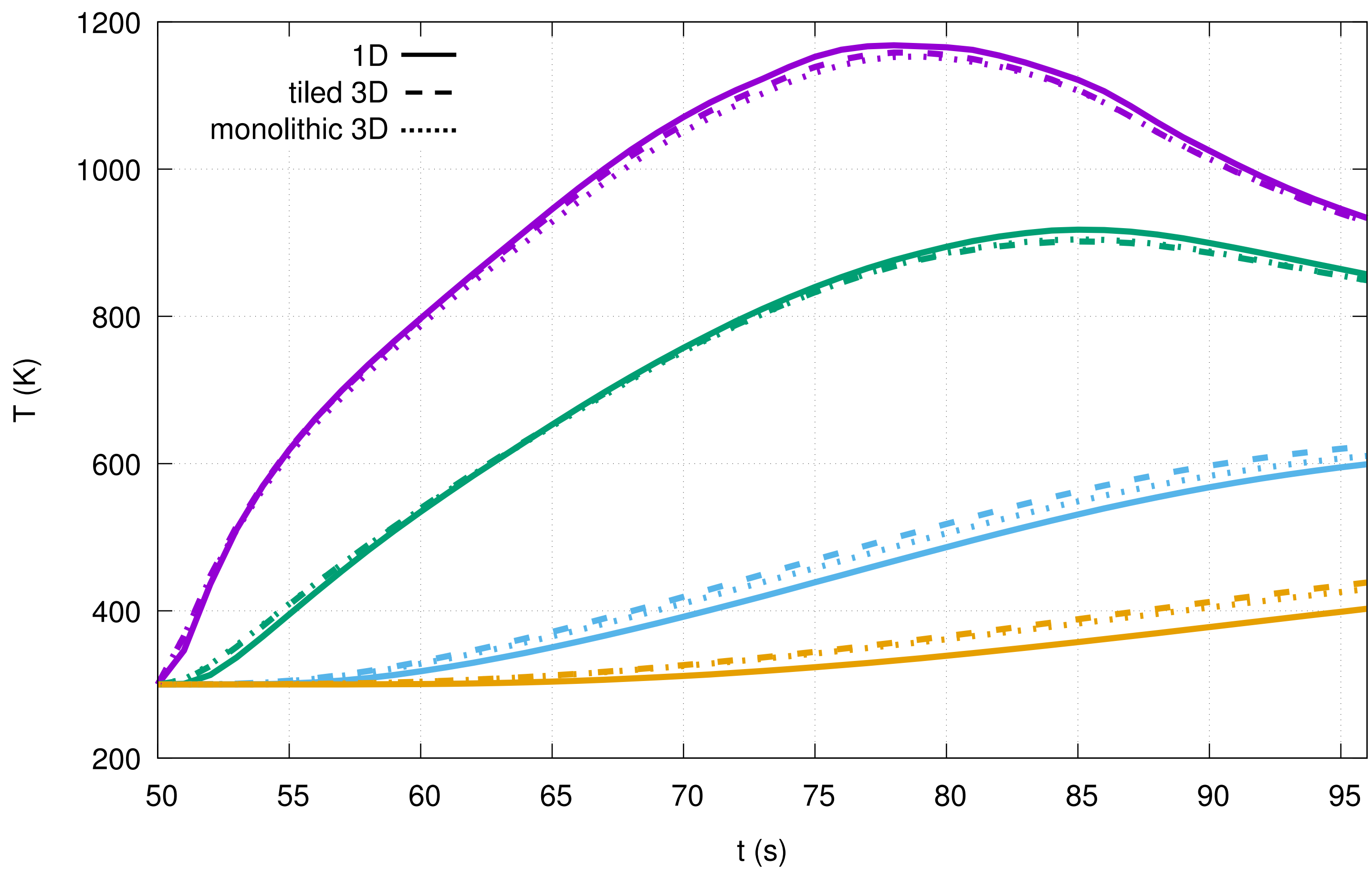

1D and 3D material response comparison – shoulder

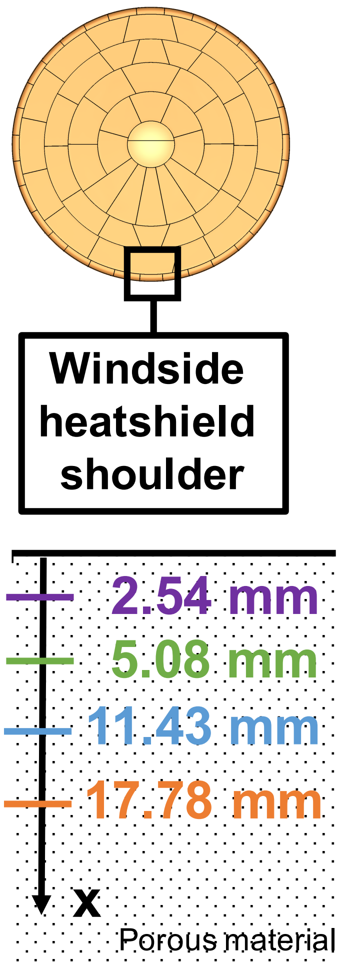

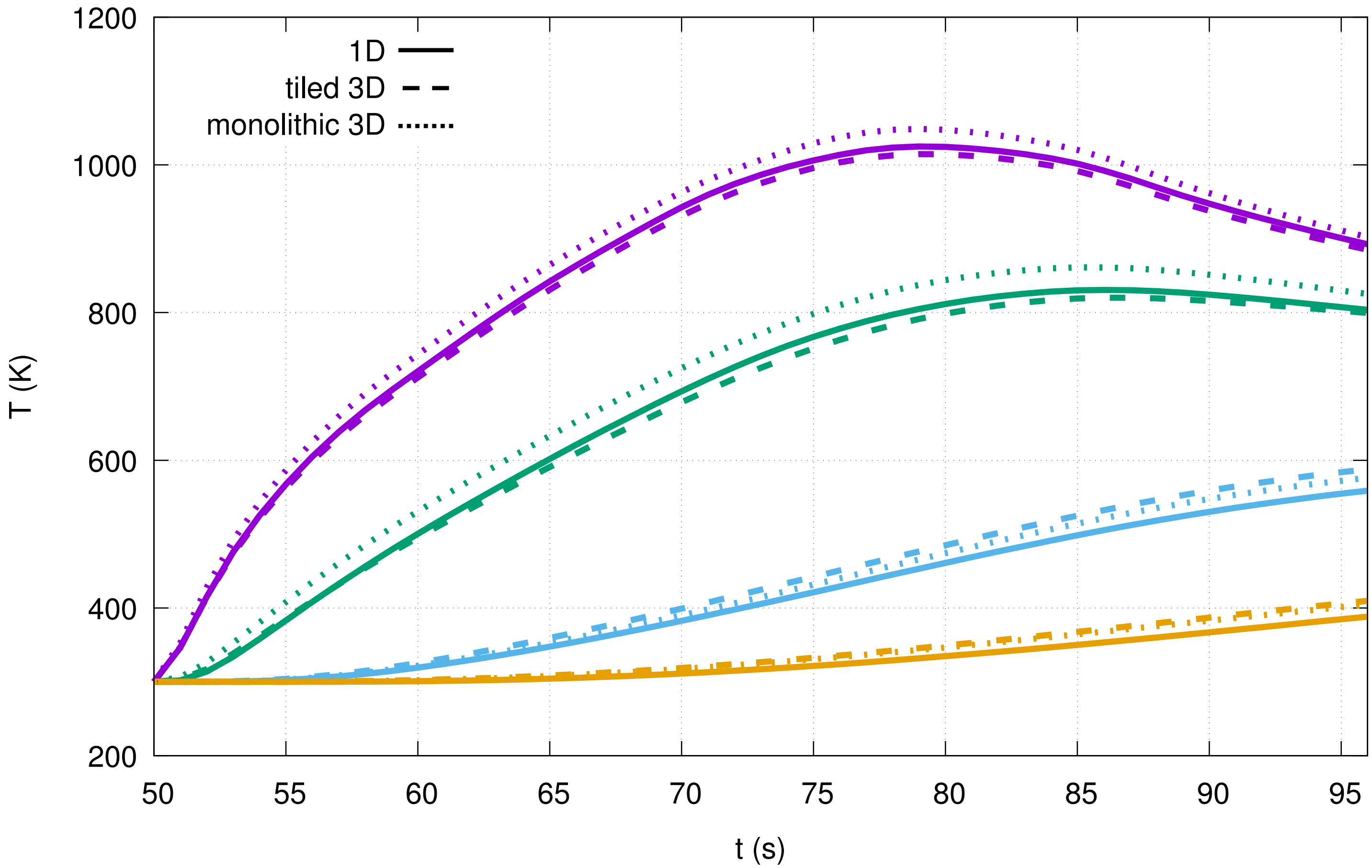

Conclusion

Hypersonic environment (DPLR)

- Laminar
- Super-catalytic wall
- Non-blowing
- 8 species & 12 reactions

Conclusion

Hypersonic environment (DPLR)

- Laminar
- Super-catalytic wall
- Non-blowing
- 8 species & 12 reactions

Porous material response (PATO)

- Pyrolysis
- CMA-type BL approx.
- No finite-rate
- Equilibrium

Conclusion

Hypersonic environment (DPLR)

- Laminar
- Super-catalytic wall
- Non-blowing
- 8 species & 12 reactions

Soft coupling

→

Linear in time
Conservative in space by local Galerkin projection

Porous material response (PATO)

- Pyrolysis
- CMA-type BL approx.
- No finite-rate
- Equilibrium

Conclusion

Hypersonic environment (DPLR)

- Laminar
- Super-catalytic wall
- Non-blowing
- 8 species & 12 reactions

Soft coupling →

Linear in time
Conservative in space by local Galerkin projection

Porous material response (PATO)

- Pyrolysis
- CMA-type BL approx.
- No finite-rate
- Equilibrium

↓ **Outputs**

- Monolithic & tiled
- Temperature 1D & 3D
- Recession 1D & 3D
- Internal velocity

Future work

Hypersonic environment (DPLR)

- Laminar
- Super-catalytic wall
- Non-blowing
- 8 species & 12 reactions

Strong coupling

Linear in time
Conservative in space by local Galerkin projection

Future work includes blowing from pyrolysis & moving mesh from recession

Porous material response (PATO)

- Pyrolysis
- CMA-type BL approx.
- No finite-rate
- Equilibrium

Outputs

- Monolithic & tiled
- Temperature 1D & 3D
- Recession 1D & 3D
- Internal velocity

Future work

Hypersonic environment (DPLR)

- Laminar
- Super-catalytic wall
- Non-blowing
- 8 species & 12 reactions

Strong coupling

Linear in time
Conservative in space by local Galerkin projection

Future work includes blowing from pyrolysis & moving mesh from recession

Porous material response (PATO)

- Pyrolysis
- CMA-type BL approx.
- No finite-rate
- Equilibrium

New technology

- 2020 mission
- Non-uniform thickness
- Transient turbulent
- MMOD & micro-scale

Outputs

- Monolithic & tiled
- Temperature 1D & 3D
- Recession 1D & 3D
- Internal velocity

New technology

PATO is capable of massively parallel computing for material response

References

[1] K. T. Edquist, A. A. Dyakonov, M. J. Wright, C. Y. Tang, Aerothermodynamic Design of the Mars Science Laboratory Heatshield, in: 41st AIAA Thermo-physics Conference, AIAA Paper 2009-4075, San Antonio, Texas, 2009. doi:10.2514/6.2009-4075.

[2] F. Panerai, J. D. White, T. J. Cochell, O. M. Schroeder, N. N. Mansour, M. J. Wright, A. Martin, Experimental measurements of the permeability of fibrous carbon at high-temperature, International Journal of Heat and Mass Transfer 101 (2016) 267 – 273.

[3] J. Lachaud, J. B. Scoggins, T. E. Magin, M. G. Meyer, N. N. Mansour., A generic local thermal equilibrium model for porous reactive materials submitted to high temperatures, International Journal of Heat and Mass Transfer 108 (2017) 1406–1417.

[4] J. B. Scoggins, T. E. Magin, Development of Mutation++: Multicomponent Thermodynamic and Transport Properties for Ionized Plasmas written in C++, in: 11th AIAA/ASME Joint Thermophysics and Heat Transfer Conference, AIAA Paper 2014-2966, Atlanta, GA, 2014.

[5] T. R. White, M. Mahzari, D. Bose, J. A. Santos, Post-flight Analysis of the Mars Science Laboratory Entry Aerothermal Environment and Thermal Protection System Response, in: 44th AIAA Thermophysics Conference, AIAA Paper 2013-2779, San Diego, CA, 2013.

[6] M. J. Wright, T. White, N. Mangini, Data Parallel Line Relaxation (DPLR) Code User Manual: Acadia-Version 4.01.

[7] M. R. Wool, Aerotherm equilibrium surface thermochemistry computer program, version 3. volume 1. program description and sample problems, Tech. rep., AEROTHERM CORP MOUNTAIN VIEW CA (1970).

[8] C. B. Moyer, M. R. Wool, Aerotherm charring material thermal response and ablation program, version 3. volume 1. program description and sample problems, Tech. rep., AEROTHERM CORP MOUNTAIN VIEW CA (1970).

[9] Y. Chen, R. Milos, Ablation and thermal response program for spacecraft heatshield analysis, Journal of Spacecraft and Rockets 36 (1999).

[10] P. Farrell, J. Maddison, Conservative interpolation between volume meshes by local galerkin projection, Computer Methods in Applied Mechanics and Engineering 200 (1) (2011) 89–100.

[11] A. Borner, F. Panerai, N. N. Mansour, High temperature permeability of fibrous materials using direct simulation monte carlo, International Journal of Heat and Mass Transfer 106 (2017) 1318 – 1326.

[12] R. A. Mitcheltree, P. A. Gnoffo, Wake flow about a MESUR mars entry vehicle, AIAA paper 1958 (1994) 1994.

[13] J.C. Ferguson, F. Panerai, J. Lachaud, A. Martin, S.C. Bailey, N.N. Mansour, Modeling the oxidation of low-density carbon fiber material based on microtomography, Carbon 96 (2016) 57–65.

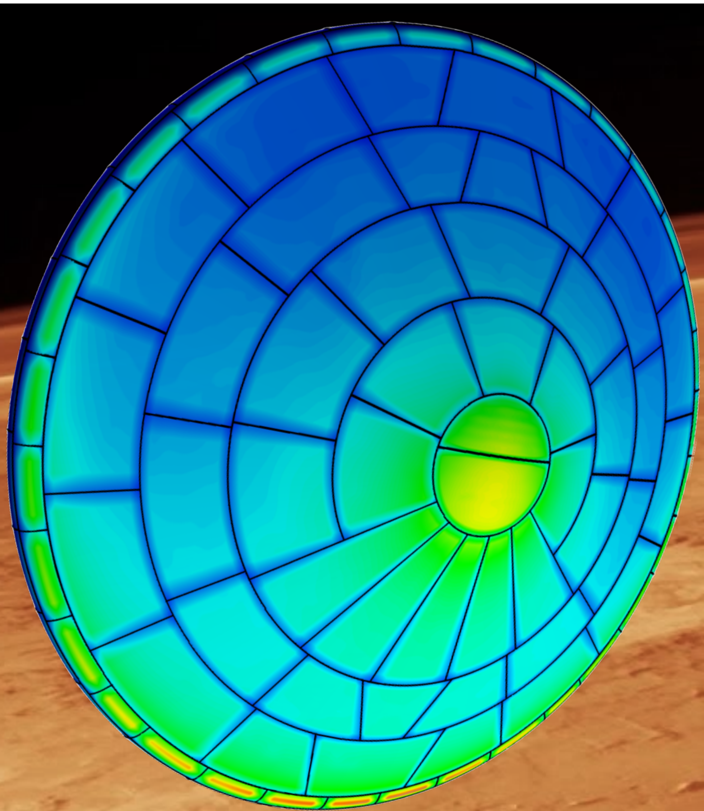

Questions ?

9th Ablation Workshop

Montana State University, August 30th - 31st, 2017

Contact
Jeremie B. E. Meurisse
(650) 604 1658
jeremie.b.meurisse@nasa.gov